A 3D Code für MHD Equilibrium and Stability

R. Chodura and A. Schlüter

IPP 1/180   March 1980

MAX-PLANCK-INSTITUT FÜR PLASMAPHYSIK

8046 GARCHING BEI MÜNCHEN

MAX-PLANCK-INSTITUT FÜR PLASMAPHYSIK

GARCHING BEI MÜNCHEN

A 3D Code für MHD Equilibrium and Stability

R. Chodura and A. Schlüter

IPP 1/180   March 1980

Abstract

A code is described which transfers an arbitrary initial plasma and field configuration under the constraints of mass and flux conservation into an equilibrium state by minimizing the energy of the system so that, in principle, the equilibrium attained is stable. Several possible minimizing algorithms are implemented and compared. One of them introduces an artificial time amd derives additional information on the lowest eigenvalue of the asymptotic linear problem from time history. Time integration of this method is explicit with time steps of varying length which admits a mean step two orders of magnitude larger than the usual stability limit.

The computation grid is Eulerian corresponding to space-fixed cylindrical coordinates whose boundary is a torus surface with rectangular cross-section. By this choice numerical flux conservation is not automatically guaranteed but it is possible to handel complicated field topologies. The code is checked against known analytical results and the dependence on the mesh size is studied. It is applied to calculate non-axisymmetric, toroidal equilibria with one or more magnetic axes and to determine the instabilities of helical $\ell = 2$ and 3 configurations.

1. Introduction

One of the basic problems of plasma physics is the calculation of general 3-dimensional magnetohydrostatic equilibria and the assessment of their stability. Knowing these is essential for designing confinement devices without ignorable coordinates such as stellarators or tokamaks disturbed by ripple, additional helical windings or instability.

The solution of this problem is approached along two lines, i.e.

a) analytically, by solving the equations for equilibrium directly, using small parameters /1,2,3/,

b) numerically, by satisfying the equilibrium conditions on a grid iteratively.

It is this latter approach which will be described here. Starting from an arbitrary distribution of plasma pressure and magnetic field, this distribution is adjusted under magnetic flux, mass and entropy conservation in such a way that the plasma energy $W = \int d^3x \left(B^2/2 + p/(\gamma - 1) \right)$ is decreased monotonically. A state of minimum energy is thus approached which represents a MHD equilibrium. To be sure that this equilibrium is a state of minimum energy with respect to all degrees of freedom, the system is displaced stochastically from this equilibrium. It now relaxes toward the old or a new equilibrium which is now definitively stable.

Previous numerical work on the minimization problem /4/ uses the set of nested magnetic flux surfaces as Lagrangian coordinate surfaces. It is thus restricted to the case of only one magnetic axis. We use a much simpler space-fixed Eulerian coordinate system which admits more than one magnetic axis to be present at the expense of the magnetic flux not being automatically attached to mass motion.

A different, but related, method /5/ follows the full plasma dynamics by solving the complete MHD equations in time in a mixed Eulerian – Lagrangian grid and approaches equilibrium by inserting a friction term into the equation of motion.

In the next section we describe the properties of the potential energy in the neighbourhood of an equilibrium. From this knowledge we derive in Sec. 3 different strategies of proceeding from an arbitrary initial state to the state of minimum energy. Section 4 describes the method of investigating stability properties of a given equilibrium. In Sec. 5 we give some details

of the numerical procedure. Section 6 shows results of tests on the reliability of the code and of calculations of different stellarator equilibria and their stability.

2. Properties of the Equilibrium

A MHD equilibrium is characterized as a stationary state of the potential energy W,

$$W = \int d^3x \left(B^2/2 + p/(\gamma - 1) \right),$$
(1)

$$\delta W = 0,$$
(2)

in respect of infinitesimal displacements $\underline{\xi}(x)$ which satisfy the constraints of mass and magnetic flux conservation, i.e.

$$\delta \rho = - \nabla \cdot \left(\rho \, \underline{\xi} \right),$$
(3)

$$\delta \underline{B} = \nabla \times \left(\underline{\xi} \times \underline{B} \right).$$
(4)

The initial state is assumed to be isentropic, and therefore one may put

$$p = \rho^\gamma$$
(5)

throughout.

The plasma is contained in a straight or toroidal domain of fixed rectangular cross-section. The plasma extends to the wall without a vacuum region in between. In the limit of very low densities the field becomes force-free rather than a vacuum field. The boundary condition at the wall is assumed to be

$$\underline{\xi} = 0.$$
(6)

The magnetic field may pass through the wall, i.e. the wall is not a flux surface, but according to eq. (6)

$$\delta \underline{B} \cdot \underline{n} = 0,$$
(7)

the normal component of the field does not change, i.e. the magnetic flux is frozen in the infinitely conducting wall.

With the aid of the constraints (3) and (4) the energy variation δW can be rewritten as

$$\delta W = - \int d^3x \; \underline{F} \cdot \underline{\xi} \tag{8}$$

where $\underline{F}$ represents the local force of the plasma

$$\underline{F} = (\nabla \times \underline{B}) \times \underline{B} - \nabla p . \tag{9}$$

The Euler equation of the variation (2) is thus the equilibrium condition of magnetohydrostatics

$$\underline{F} = 0 . \tag{10}$$

If $\underline{\xi}$ is a small displacement starting from an equilibrium state, then $\underline{F}$ is linear and δW is quadratic in $\underline{\xi}$ because of eq. (8):

$$\underline{F}(\underline{\xi}) \propto \underline{\xi} \quad , \quad \delta W = - \frac{1}{2} \int d^3x \; \underline{F}(\underline{\xi}) \cdot \underline{\xi} . \tag{11}$$

In order to illustrate the structure of W near the equilibrium, one may assume $\underline{\xi}$ to be expanded in terms of discrete eigenfunctions of the linear operator $\underline{F}$

$$\frac{1}{\rho} \underline{F}(\underline{\xi}_i) = - \lambda_i \underline{\xi}_i \tag{12}$$

with normalization

$$\int d^3x \; \rho \; \underline{\xi}_i^2 = 1 , \tag{13}$$

$$\underline{\xi} = \sum_i a_i \underline{\xi}_i .$$

Equation (11) may then be rewritten as

$$\delta W = \frac{1}{2} \sum_i a_i^2 \lambda_i \tag{14}$$

In the space of eigenfunctions the cut $W = $ const for $\lambda_i > 0$ is thus an ellipsoid with halfaxis proportional to $\lambda_i^{-1/2}$ (Fig. 1). Since the eigenvalues which are represented in the numerical grid differ by many orders of magnitude the ellipsoid contains long and flat as well as short and steep portions and both have to be resolved on the path of convergence to the minimum of W.

3. Routes to the Energy Minimum

We start with an arbitrary distribution of density ρ and magnetic field $\underline{B}$ with $\nabla \cdot \underline{B} = 0$ as initial state. Let us describe a path of displacement to the energy minimum by $\underline{\xi}(t)$ where t is a time-like parameter. We can then define a "velocity" $\underline{v}$ by

$$d\underline{\xi} = \underline{v} \, dt \tag{15}$$

and transform the constraints (3) and (4) into differential equations in t,

$$\partial \rho / \partial t = - \nabla \cdot (\rho \underline{v}), \tag{16}$$

$$\partial \underline{B} / \partial t = \nabla \times (\underline{v} \times \underline{B}). \tag{17}$$

Equation (8) now becomes

$$d W / dt = - \int d^3x \; \underline{F} \cdot \underline{v} \tag{18}$$

a) Friction Model (MHF)

A possible way of approaching the minimum potential energy is given by /6, 7/

$$\underline{v}(\underline{x}, t) = \alpha \underline{F}(\underline{x}, t) \tag{19}$$

where α is a positive number, function or operator (Fig. 1, Curve 1). According to eq. (18) differential displacements (19) lead to a steady diminuation of W.

The set of equations (9), (16) and (17) together with the assumption (19) is a parabolic system. It describes the motion of a plasma under the action of a friction force $\alpha^{-1} \underline{v}$ without inertia. The friction force steadily extracts energy and the plasma creeps into an equilibrium state.

b) Gradient Method

This method is different from the preceding one in that it proceeds, in principle, in discrete steps. At the beginning of step n at time t_n the direction of displacement $\underline{v}_n$ is calculated from equ. (19),

$$\underline{v}_n = \alpha \underline{F}_n, \tag{20}$$

which guarantees decreasing energy at the start. This direction is maintained during the whole step, i.e. the displacement ξ is given by

$$\xi = \xi_n + \underline{v}_n \, (t - t_n). \tag{21}$$

According to eq. (11) for this displacement and in the neighbourhood of an equilibrium W decreases quadratically with time towards a minimum. The time when this minimum is reached, t_{n+1}, can be determined by calculating the derivatives

$$\dot{W} = -\int d^3x \, \underline{F} \cdot \underline{v}$$

at t_n and at a test time t_s, $\dot{W}_n$ and $\dot{W}_s$ respectively:

$$t_{n+1} = t_n + a \dot{W}_n \, (t_s - t_n) / (\dot{W}_n - \dot{W}_s) \, , \quad a \approx 1 \tag{22}$$

In practice, it is necessary to stop slightly before the minimum, e.g. at $a = 0.8 \ldots 0.9$ of the ideal step time. Otherwise the iteration would fall into cycles of two orthogonal displacements within the same "plane", leading to very poor convergence (Fig. 2). At the end of the step the new direction v_{n+1} is calculated from eq. (20) (which is nearly perpendicular to the preceding one), and the next step along this new direction is executed (Fig. 1, Curve 2).

In the course of iteration there will occur steps where the system by chance moves nearly along an eigenmode of αF with eigenvalue λ. The time length of such a step is $1/\lambda$. Thus from the minimum occuring step length the largest eigenvalue λ_{Max} and the admissible time step Δt_0 of eq. (33) can be derived.

c) Conjugate Gradient Method

This method improves the gradient method by determining the minimum of W not only along a fixed "line" with direction $\underline{v}_n$ but within a "plane" built by the direction of displacement during the preceding step v_{n-1} and the force at the beginning of the new step $\underline{F}_n$ (Fig. 1, Curve 3):

$$\underline{v}_n = \underline{F}_n + b \, \langle F_n^2 \rangle / \langle F_{n-1}^2 \rangle \, \underline{v}_{n-1} \tag{23}$$

Here $\underline{F}_{n-1}$ is the force at the beginning of the preceding step and $\langle \, \rangle$ means an average over the whole volume. By proceeding from time step to time step an increasing number of dimensions in Hilbert space is thereby included in the minimization procedure so that after a number of steps equal to the number of eigenvalues of $\underline{F}$ the absolute minimum of W would be reached if numerical errors were absent and if the "nonlinear" effect were negligible. The convergence rate of this method is very sensitive to the numerical factor b in eq. (23) which should be slightly smaller than 1 (i.e. $b = 0.999 \ldots 0.998$) for optimal convergence.

Fig. 2 compares the convergence towards equilibrium for the three methods as given by the residual force $\langle F^2 \rangle$. The friction method is considerably improved by a method of varying time steps as described in section 5b. It then gives, together with the conjugate gradient method, the best results.

4. Stability

The state of lowest energy, which is approached by minimizing the potential energy W, is, in principle, a stable equilibrium. Nevertheless it may be that the final state of an iteration may not be the state of lowest energy if unstable modes of this final state had not been excited in the course of iteration. If, for instance, the initial state was axisymmetric it will stay so during the minimization process and the final state will be axisymmetric, too. This equilibrium may be unstable in respect of non-axisymmetric modes.

Therefore, in order to be sure that a final state is really a state of lowest energy, one has to excite all degrees of freedom of the system, i.e. all eigenmodes. This is achieved by disturbing the final state either in an ordered fashion by a Fourier mode or more or less stochastically (Fig.9). If the state was stable, the energy W, after rising with the disturbance, will return to its previous value; if it was unstable the energy will decrease to a lower level (Fig.3).

Furthermore, using the MHF method one can obtain the lowest eigenvalue of this equilibrium from the time behaviour of the approximation toward the equilibrium. To show this, we compare the MHF model with the usual MHD:

MHD   MHF

$$\text{Assume} \quad \alpha = \left(\mu \, \varsigma \right)^{-1}, \quad \mu = const. \quad (24)$$

The linearized equation of motion

$$\varsigma_0 \, \partial^2 \underline{\xi} / \partial t^2 = \underline{F}\left(\underline{\xi}\right) \qquad \mu \varsigma_0 \, \partial \underline{\xi} / \partial t = \underline{F}\left(\underline{\xi}\right) \qquad (25)$$

can be solved by the separation ansatz

$$\underline{\xi} = \hat{\underline{\xi}}\left(\underline{x}\right) e^{\omega t} \qquad (26)$$

which leads to the eigenvalue equation

$$\frac{1}{\varsigma_0} \, \underline{F}\left(\hat{\underline{\xi}}_k\right) = -\lambda_k \, \hat{\underline{\xi}}_k, \qquad \lambda_k \; \text{real} \qquad (27)$$

Thus, the time behaviour of the solution is given by

$$\omega^2_k = -\lambda_k , \qquad\qquad \mu \, \omega_k = -\lambda_k , \qquad\qquad (28)$$

$$\xi = \sum_k c_k \, \hat{\xi}_k (\underset{\sim}{x}) \, e^{i\sqrt{\lambda_k}\, t} , \qquad\qquad \xi = \sum_k c_k \, \hat{\xi}_k (\underset{\sim}{x}) \, e^{-\lambda_k t / \mu} \qquad (29)$$

i.e. while MHD modes are either oscillating or exponentially growing, MHF modes are either exponentially damped or growing. In the course of time the mode with the lowest eigenvalue will dominate the MHF spectrum. Thus, from the asymptotic time behaviour of, for instance, $\langle F^2 \rangle$ in the vicinity of the equilibrium, the lowest eigenvalue can be derived. Equations (28) then give the eigenfrequency of the corresponding lowest MHD eigenmode. For any choice of $\alpha > 0$ at least the marginal points of stability are the same for MHF and MHD.

5. Numerical Procedure

a) Spatial Discretization

The process of energy minimization is performed in a space-fixed Eulerian grid. Cylindrical coordinates around the torus axis are used which may degenerate to Cartesian coordinates for a straight configuration.

In order to conserve mass and flux over an elementary cell we define different variables on different points of the cell (Fig. 4), i.e. the mass of the cell M at the centre of the volume, the magnetic fluxes ψ_x, ψ_y, ψ_z, and mass fluxes at the midpoints of the corresponding surfaces and electric field components $\underline{E} = -\underline{v} \times \underline{B}$ at midpoints of corresponding edges. By this choice for the location of variables the changes of mass and magnetic fluxes in the cell and through its walls can easily be calculated by using Gauss's and Stoke's theorems respectively. The total mass of all cells is conserved and the sum of the magnetic fluxes through all surfaces of a cell stays at zero.

The most important point is the discretization of the force $\underline{F}$. Force and velocity are defined at vertices of the cell. We start from an approximation to the energy of the system, assuming the magnetic field $\underline{B}$ to vary linearly between mesh points:

$$W = \sum_{ijk} \left\{ 1/6 \left[B_x^2(i+1/2, j, k) + B_x^2(i-1/2, j, k) + B_x(i+1/2, j, k) B_x(i-1/2, j, k) \right. \right.$$
$$\left. + (x \rightarrow y) + (x \rightarrow z) \right]$$
$$\left. + p^{\gamma}(i, j, k)/(\gamma - 1) \right\} \Delta V(i, j, k) \tag{30}$$

Deriving W with respect to t and inserting the discretized form of conservation equation (16) and (17), we get an expression for $\dot{W}$ which is linear in $\underline{v}$. Collecting all terms with $v_x(\underline{J})$, $v_y(\underline{J})$, $v_z(\underline{J})$, where $\underline{J}$ stands for $(i+1/2, j+1/2, k+1/2)$, we can with eq. (18) identify their coefficients with the force components $- F_x(\underline{J})$ $- F_y(\underline{J})$, $- F_z(\underline{J})$. This choice of $\underline{F}$ implies satisfaction of eq. (18) in the space-descretized form

b) Discretization in Time

For calculating the change of p and $\underline{B}$ in time from eqs. (16) and (17) for fixed $\underline{v}$, we use an explicit second-order integration scheme. While the gradient and conjugate gradient methods use time steps which are automatically stable, the MHF method has to consider a maximum admissible time step Δt_o for numerical stability. This time step is determined by the largest eigenvalue λ_{Max} of the operator $\alpha \underline{F}$:

Since for the mode with eigenvalue λ

$$(\xi^n - \xi^{n-1})/\Delta t = \alpha F(\xi^{n-1}) = -\lambda \xi^{n-1}, \tag{31}$$

the amplification factor V of ξ at subsequent time steps n and $n-1$, $\xi_n = V \xi_{n-1}$, is given by

$$V = 1 - \lambda \Delta t \tag{32}$$

(as compared with the correct value $e^{-\lambda \Delta t}$ for the differential form of eq. (31)) and since one requires $|V| < 1$ for numerical stability, we get the usual condition for Δt_o:

$$1 - \lambda_{Max} \Delta t_o = -1, \quad \Delta t_o = 2/\lambda_{Max} \tag{33}$$

In order to use eq. (33), one has to estimate the largest eigenvalue of the MHF system on a grid. For large eigenvalues, i.e. for short wavelengths perpendicular to the field (as compared with all gradients) the

approximate eigenvalue equation is

$$\alpha \underline{F}(\underline{\xi}) \approx \alpha \rho V_A^2 \, \partial^2 \xi / \partial x^2 = -\lambda \xi \quad , \tag{34}$$

where V_A is the magnetosonic speed, $\rho V_A^2 \approx \gamma p + B^2$. The eigenvalues λ on a grid with mesh size Δx are

$$\lambda = \alpha \rho \lambda_m = 2 \alpha \rho \left(V_A / \Delta x \right)^2 \left[1 - \cos \left(\pi \, m \, \Delta x / L \right) \right] \tag{35}$$

(Fig. 5), where L is the length of the computation interval and

$$1 \le m \le M = L / \Delta x \quad .$$

The largest eigenvalue in the grid is thus

$$\lambda_{Max} = 4 \alpha \left(\gamma p + B^2 \right)_{Max} / \left(\Delta x \right)^2 \tag{36}$$

(An automatic procedure to determine λ_{Max} and Δt_0 is given in Section 3b).
Δt_0 formally depends on the magnitude of α but the relevant quantity $\Delta \xi = \underline{v} \, \Delta t_0 =$
$= \alpha \underline{F} \, \Delta t_0$ does not. For α independent of ρ Δt_0 depends on ρ
only via p , for $\alpha \propto \rho^{-1}$ it depends on the lower bound of ρ as in MHD.
It is possible to go far beyond the admissible time step Δt_0 by using periodic sequences
of time steps with different lengths /8, 9,10/. With N being the number of time steps of the
sequence the amplification factor after the N steps for a mode with eigenvalue λ is

$$V_N = \prod_{\nu = 1}^{N} \left(1 - \lambda \Delta t_\nu \right) . \tag{37}$$

Again, for numerical stability $|V_N| < 1$ is required. One can consider V_N as a
polynomial of order N in λ with zeros $\lambda_\nu = 1 / \Delta t_\nu$ and derivative $dV_N / d\lambda = -\sum_{\nu=1}^{N} \Delta t_\nu$
at $\lambda = 0$. The polynomial of order N which decreases fastest for x=0 and is bounded between
-1 and $+1$ for arguments $0 \le x \le 2$ is the Chebychev polynomial $T_N(x-1)$ (Fig. 6).
The zeros of the polynomial are given by

$$x_\nu = 1 + \cos \left[(2\nu - 1) \pi / (2N) \right] , \quad \nu = 1, \dots N \tag{38}$$

From $x \propto \lambda$ and $x_{Max} = 2$

it follows that

$$x = 2\lambda / \lambda_{Max} = \lambda \Delta t_0$$

and

$$\Delta t_\nu = 1 / \lambda_\nu = \Delta t_0 / x_\nu \tag{39}$$

Equation (39) was derived on the assumption of linearity and hermiticity of αF. As these conditions are not strictly fulfilled and due to round-off errors it is advisable to relax V_N to a modified Chebychev polynomial $\widetilde{T}_N$ with amplitude smaller than 1 and nodes $x_\nu + \varepsilon$, $\varepsilon > 0$ (Fig. 6). This leads to time steps

$$\Delta t_\nu = \Delta t_o / (x_\nu + \varepsilon) , \qquad (40)$$

where ε and N can be decreased and increased respectively in approximating the equilibrium. For reasons of numerical stability, the Δt_ν should not be used in their natural monotonic order, but long time steps should be mixed with short ones. We got good results by choosing N as a prime number and putting $\nu = kj$, with $j = 1, 2 \cdots N$ and $k \approx N/3$. The gain of using time steps from eqs. (39) and (40) as compared with equal time steps according to eq. (33) is (for large N)

$$\langle \Delta t \rangle / \Delta t_o \approx N \qquad \text{where} \qquad \langle \Delta t \rangle = \left(\sum_{\nu=1}^{N} \Delta t_\nu \right) / N$$

and ε was chosen as $\varepsilon = O(N^{-2})$, (Fig. 2).

$$(41)$$

For large values of N it is necessary to reduce error propagation and round-off errors by calculating with double precision. Cycles of length N up to 307 have been successfully applied.

One can use still larger time steps if the spectrum λ_m of eq. (35) is changed so that the highest eigenvalue λ_{Max} is lowered while small (physical) eigenvalues stay unchanged. This is achieved by, for instance, a smoothing procedure for $\underline{V}$ which replaces $\underline{V}$ at a grid point by a weighted mean over its neighbours in the poloidal plane with relative weights

$$
\begin{array}{ccc}
1 & 2 & 1 \\
2 & 4+\varepsilon & 2 \\
1 & 2 & 1
\end{array}
\qquad (42)
$$

This smoothing results in a dispersion relation

$$\lambda_m = 2 \left(v_A / \Delta x \right)^2 \left\{ \sin^2 \left(\pi m / M \right) + \varepsilon \left[1 - \cos \left(\pi m / M \right) \right] \right\} / \left(2 + \varepsilon \right) \quad (43)$$

(Fig. 5), which cuts down λ_{Max} to about 1/2 the value of eq. (36) and thus increases Δt_o by a factor of 2.

The admissible time step Δt_o is determined by v_A^2, i.e. the eigenvalue for a wave vector perpendicular to the magnetic field. The eigenvalue along the field, on the other hand, is by a factor $c_s^2/v_A^2 \sim \beta$ (where c_s is the sound velocity) smaller than the eigenvalue perpendicular to the field. It is therefore advantageous to use an anisotropic friction coefficient with

$$\beta \, \alpha_{\parallel} \sim \alpha_{\perp} \tag{44}$$

in order to put both eigenvalues on the same scale and accelerate the parallel motion.

c) Symmetry

Many helical, toroidal, i.e. stellarator, configurations possess a symmetry of double reflection on the equatorial and a poloidal plane. This symmetry is included in the program as an option in order to save storage and computing time.

6. Tests

The most important point for testing the code was to check the dependence of the results, i.e. equilibria and lowest eigenvalues, on the grid size.

To do so, we introduced a known analytic equilibrium, i.e. an axisymmetric toroidal Solovev equilibrium /11/ as an initial condition for the iteration procedure. Owing to the discretization errors it is not an exact equilibrium on the grid, and so the code displaces the system to some extent. Fig. 7 shows the analytic equilibrium together with that of the code (for a 10 x 10 point grid) and the r.m.s. displacement from analytic equilibrium by the code for different mesh sizes The displacement decreases quadratically with the mesh size.

A similar test was performed for a 3-dimensional force-free field $(\nabla \times \underline{B}) \times \underline{B} = 0$ /12/. Again, for this field and p = const as initial conditions the code holds this equilibrium situation fixed.

Fig. 8 shows the result of a test on flux conservation. A straight helical $\ell = 2$ vacuum field is bent into a torus and filled with plasma. The plasma pressure shifts the magnetic axis outward towards an equilibrium position. In the initial state the rotational transform ℓ is nearly constant for all flux surfaces. If the code were ideally flux conserving ℓ should be conserved.

As may be seen, there is an appreciable deviation from flux conservation for rough grids, becoming small for a 20 x 20 x 20 grid.

As was pointed out in Section 4 the stability properties of an equilibrium may be tested by launching a disturbance. The disturbance may be a Fourier mode which is similar to a suspected lowest eigenvalue mode (i.e. same poloidal and axial periodicity) or it may be completely stochastic. In any case, after some time the mode with the lowest eigenvalue should evolve out of the sea of slower growing or faster damping modes. This is shown in Fig. 9 for a straight $\ell = 2$ stellarator configuration.

Another test studies the unstable eigenvalues of a straight cylinder with constant axial current density j_z = const and constant axial magnetic field B_z = const, which implies constant pitch $B_\theta / (r B_z)$ = const. Growth rates from the code of an m = 1 instability for different axial wave numbers k are plotted in Fig.10 for different grid sizes together with the theoretical curve for $B_\theta \ll B_z$ /13/. As may be noticed, the mode grows more slowly in the coarse grid and the maximum growth rate is shifted towards smaller wavelengths. Neverthe- less, by refining the grid, the true eigenvalue is approximated rather closely.

7. Results

In Fig. 11 we have plotted the flux lines for 3 cuts of a toroidal $\ell = 2$ stellarator. The flux lines are found by integrating the magnetic field lines and marking the intersection points with the given plane. The figures in the first line give the initial situation, which is a $\ell = 2$ straight vacuum field bent into a torus. Filling in an axisymmetric plasma with $\beta = 2 p_{max} / B_{z_0}^2$ results in a deformation and a shift of the flux lines and a helical distortion of the magnetic axis until the equilibrium as given in the second line is reached. The shift of the magnetic axis δ (averaged over a helical period) depends on ß, the aspect ratio A and the rotational transform ι. According to a theoretical calculation by Solovev and Shafranov /14/ this dependence can be expressed by one parameter β / β_{crit}, where $\beta_{crit} = 2 \iota^2 / A$. We have compared in Fig. 12 the shifts of our numerically calculated equilibria for A = 5 and 20, ι = 0.13 ... 0.55 and ß up to 0.25 with this theoretical prediction. The calculated points lie below the theoretical curve. This may be due to the different boundary conditions.

As was pointed out ,the main advantage of a Eulerian grid is the possibility of including more than one magnetic axis in the calculation area. The equilibrium state of a configuration with an x-point and two magnetic axes, i.e. the so-called "double star" configuration /15/ shown in Fig. 15 for A = 16 and ß = 0.03. This configuration is a superposition of a quadrupole field on a $\ell = 3$ helical field. In this configuration the toroidal shift is strongly reduced as compared with Fig. 12.

Finally, we used the code to study the stability of straight and toroidal helical confi-gurations. Fig. 14 shows the unstable m = 1, $k = 0$ eigenmode of a straight $\ell = 2$ and $\ell = 3$ equilibrium respectively. The initial disturbance with azimuthal and axial wave number m and k becomes modified by the helicity of the equilibrium. The growth rate of this mode γ turns out to decrease slightly with decreasing mesh size (Table 1).

We also investigated the growth rate γ of an unstable m = 2, $k = h/5$ flute mode of a straight helical $\ell = 2$ equilibrium with N = 5 periods, wave number $h\,a = 0.68$ and constant rotational transform t per period. γ should be largest if the pitch of the mode and of the field lines coincide, i.e. $k_{res}/(m\,h) = t_{res}$. In Fig. 15 t is varied keeping the wave number of the mode, $k = h/5$, fixed. By increasing the number of mesh points the resonance curve approaches its correct position and the growth rates increase. The extrapolated curve for $\Delta x = 0$ was obtained by assuming a $(\Delta x)^2$-dependence of the eigenvalue γ^2 on grid size Δx for $\Delta x \to 0$.

$$\gamma^2 / (v_A /a)^2 \times 10^4$$

$(\Delta x)^2$	$\ell = 2$	$\ell = 3$
0.028	4.8	
0.020	4.6	
0.016	3.8	4.7
0.010	3.4	4.0

Table 1   Growth rates γ of straight helical $\ell = 2$ and 3 configurations with ß = 0.5 for different grids $(v_A^2 = B_{zo}^2 / \rho_{Max})$

If the $\ell = 2$ helix is bent into a torus, keeping the length of the helix and of the disturbance fixed, the eigenvalues of the new equilibrium are shifted towards stability as compared with the straight case. In a $20^2 \times 100$ mesh grid the resonant mode appears stable for aspect ratios A (for pressure 1/e-width) below 30, and the maximum eigenvalue at A = 60 has about half the value of the corresponding straight case (A = ∞) (Fig. 16). For smaller grid sizes the aspect ratio for marginal stability may be expected to be smaller.

Conclusion

The 3D Eulerian code described is capable of finding the equilibrium state to a given initial distribution of field and pressure and to assess its stability. Grids with more than 14^3 mesh points are necessary if one wants to achieve quantitatively correct results.

Acknowledgement

References

/1/   D.C. Barnes et al., Proc. 7th IAEA Conf. on Plasma Physics and Controlled
Nucl. Fusion Res., Innsbruck (1978), Vol.2, p. 345

/2/   D. Lortz, J. Nührenberg, Proc. 7th IAEA Conf. on Plasma Physics and
Controlled Nucl. Fusion Res., Innsbruck (1978), Vol.2, p. 309

/3/   G.O. Spies, Nucl. Fusion 18 (1978), 1671

/4/   F. Bauer, O. Betancourt, P. Garabedian, "A Computational Method in Plasma
Physics", Springer, New York/Heidelberg/Berlin, 1978

/5/   D.C. Barnes, J.U. Brackbill, Nucl. Sci. and Engr. 64 (1977), 18

/6/   A. Schlüter, Sitzungsberichte der Bayer. Akademie d.Wissenschaften,
München 1975, Nr. 11

/7/   A. Schlüter, R. Chodura, Proc. 3rd Topical Conf. on Pulsed High Beta Plasmas,
Culham, 1975 (D.E. Evans Ed.), p. 187

/8/   P. Merkel, A. Schlüter, Sitzungsbericht der Bayer. Akademie d. Wissenschaften,
München 1976, Nr. 7

/9/   R. Chodura, A. Schlüter, Proc. 2nd European Conf. on Computational Physics
in Plasmas, Garching, 1976 (D. Biskamp Ed.), C2

/10/ W. Gentzsch, A. Schlüter, ZAMM 58, T 415 (1978)

/11/ L.S. Solovev, ZhETF 53 (1967) 626; Sov. Phys. JETP 26 (1968)

/12/ F. Cap, D. Lortz, J. Nührenberg, private communication

/13/ J.P. Goedbloed, H.J.L. Hagebeuk, Phys. Fluids 15 (1972),1090

/14/ L.S. Solovev, V.D. Shafranov, Reviews of Plasma Physics (M.A. Leontovich ed.),
vol. 5, p. 127, Consultants Bureau New York/London, 1970

/15/ T. S. Wang, T.H. Jensen, Nucl. Fusion 18 (1978) 1459
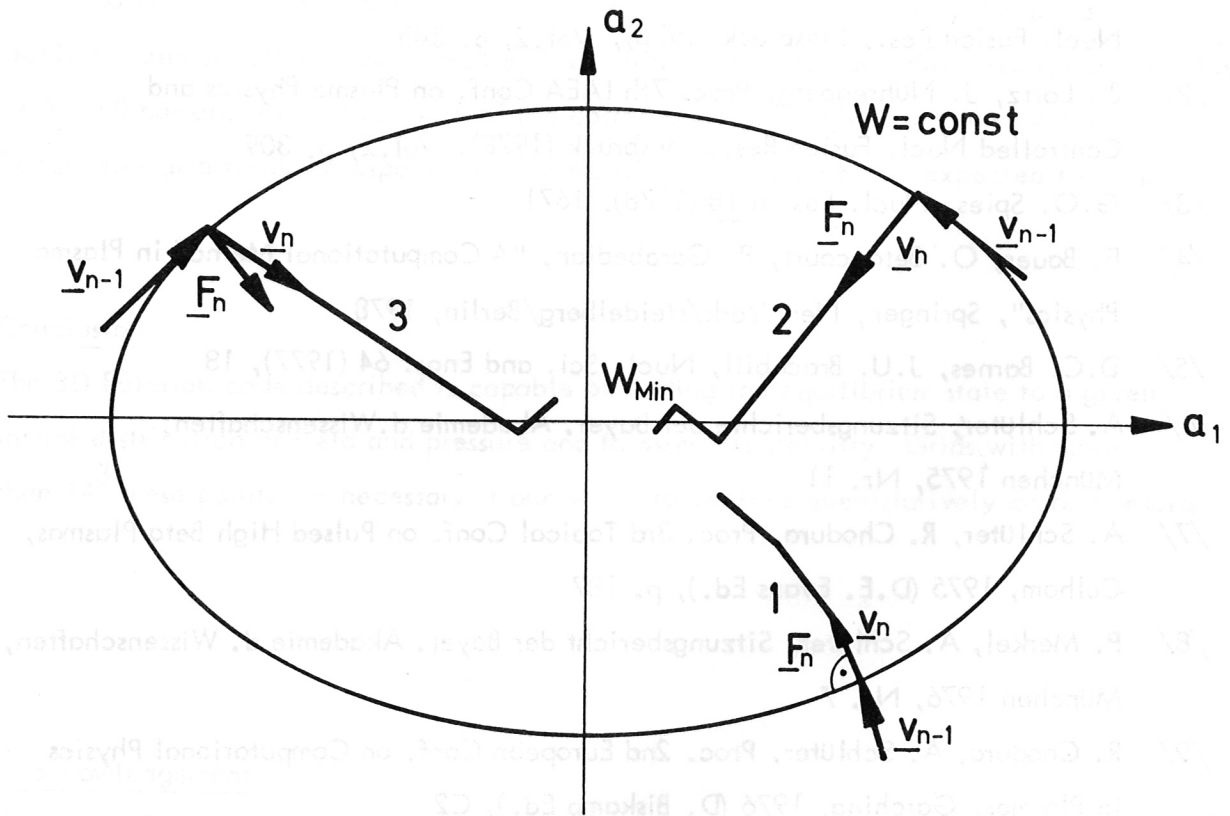
1 Friction method
2 Gradient method
3 Conjugate gradient method

Fig. 1 Schematic picture of paths of convergence W_{min} using different iteration methods. For simplicity the system is assumed to have only two eigenstates.
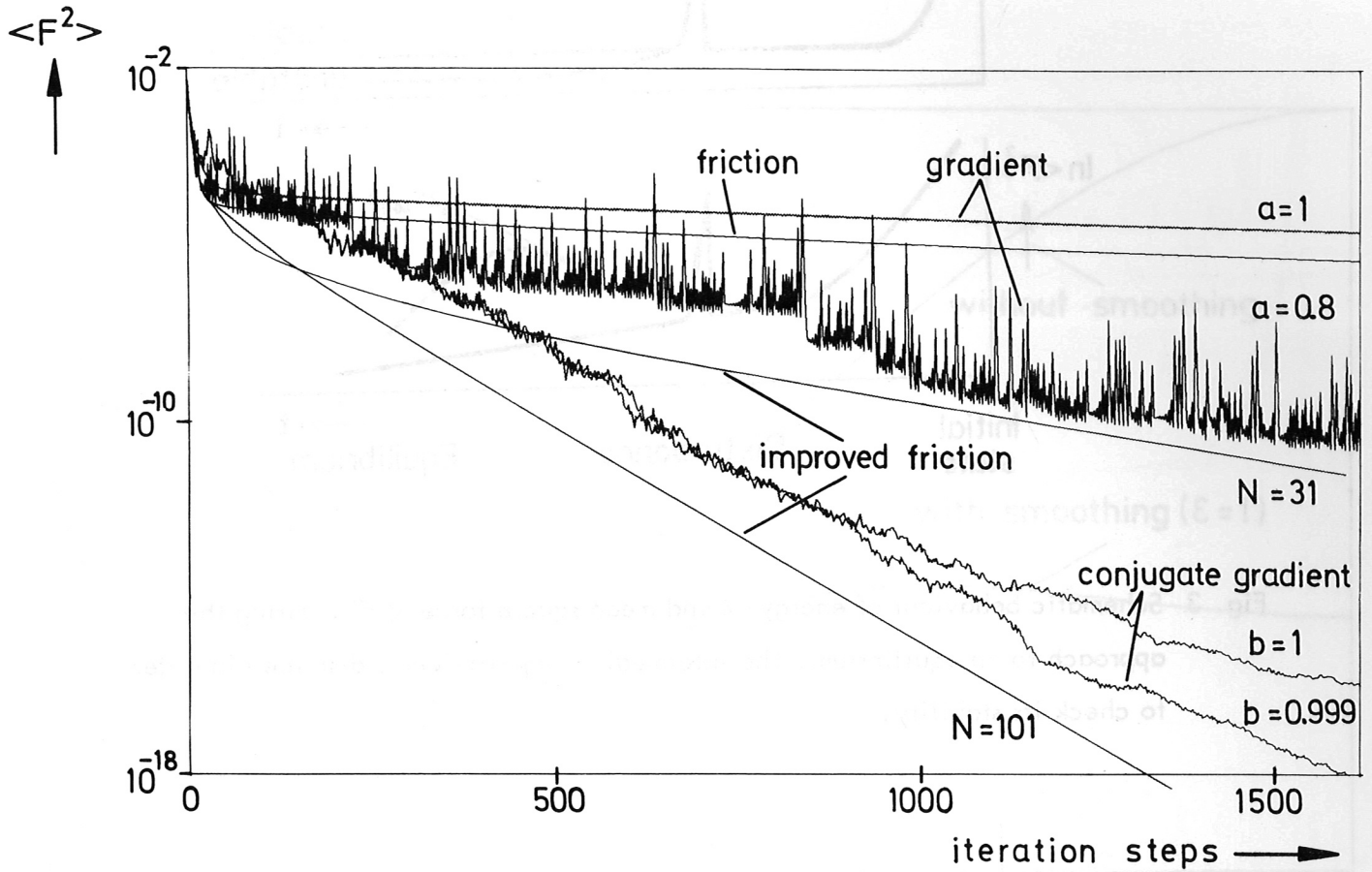
Fig. 2 Convergence rate for different iteration methods

1. Friction method with equal time steps

2. Friction method with periodic sequence of N unequal time steps according to eq. (40)

3. Gradient method with different fractions a of the step length to the minimum (a = 1 and 0.8)

4. Conjugate gradient method with different weight coefficients b = 1 and 0.999.
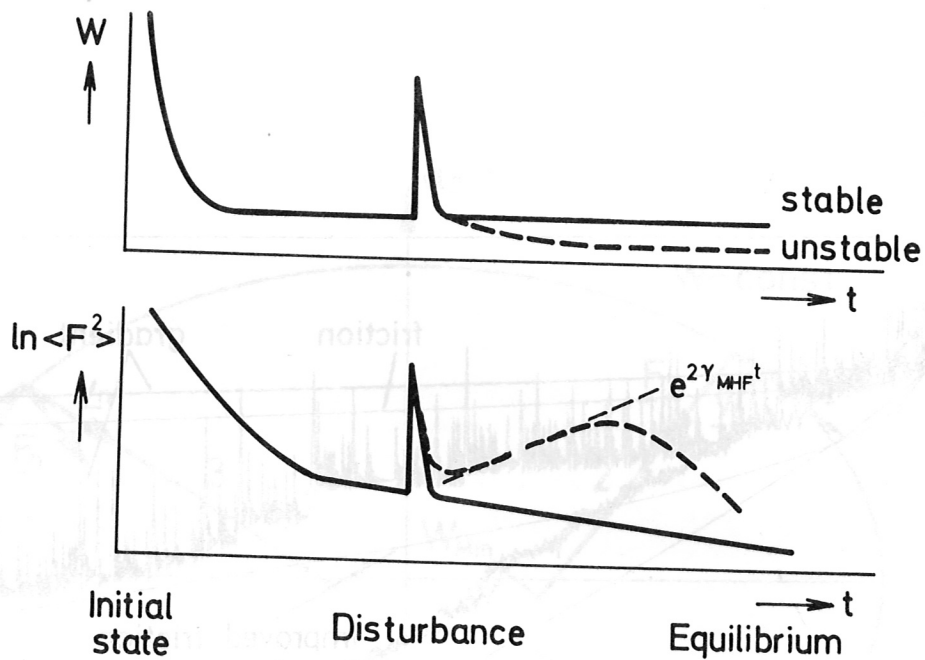
Fig. 3 Schematic behaviour of energy W and mean square force $\langle F^2 \rangle$ during the approach to an equilibrium. The intermediate equilibrium is disturbed in order to check its stability.
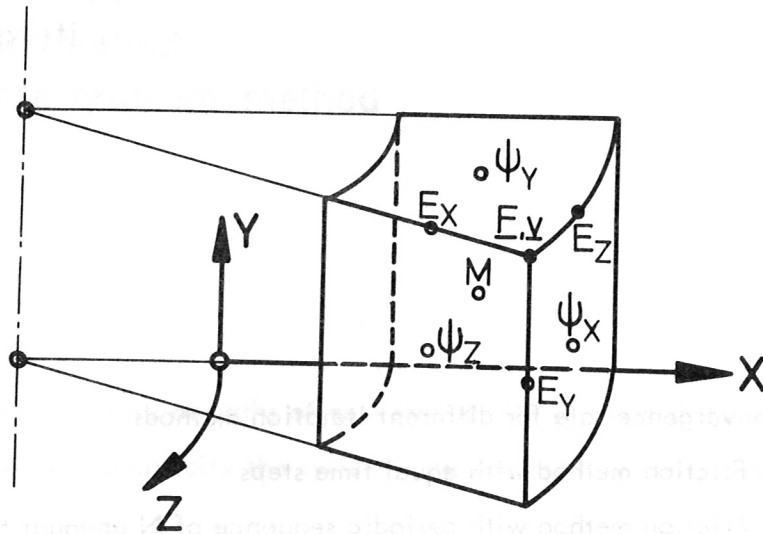
Fig. 4 Elementary cell of calculation grid with location of the variables.
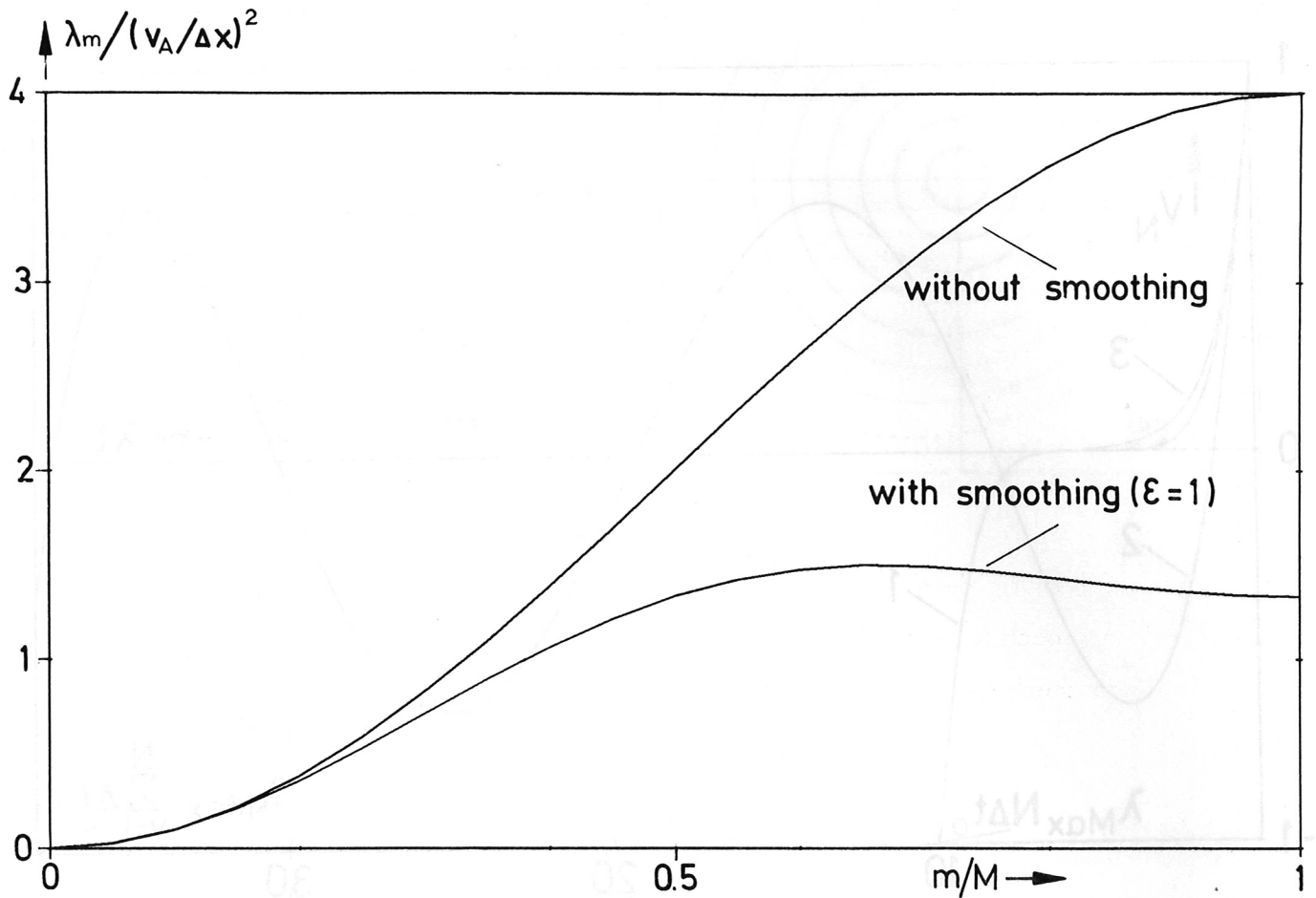
Fig. 5 Eigenvalue λ_m for mode numbers $m \gg 1$
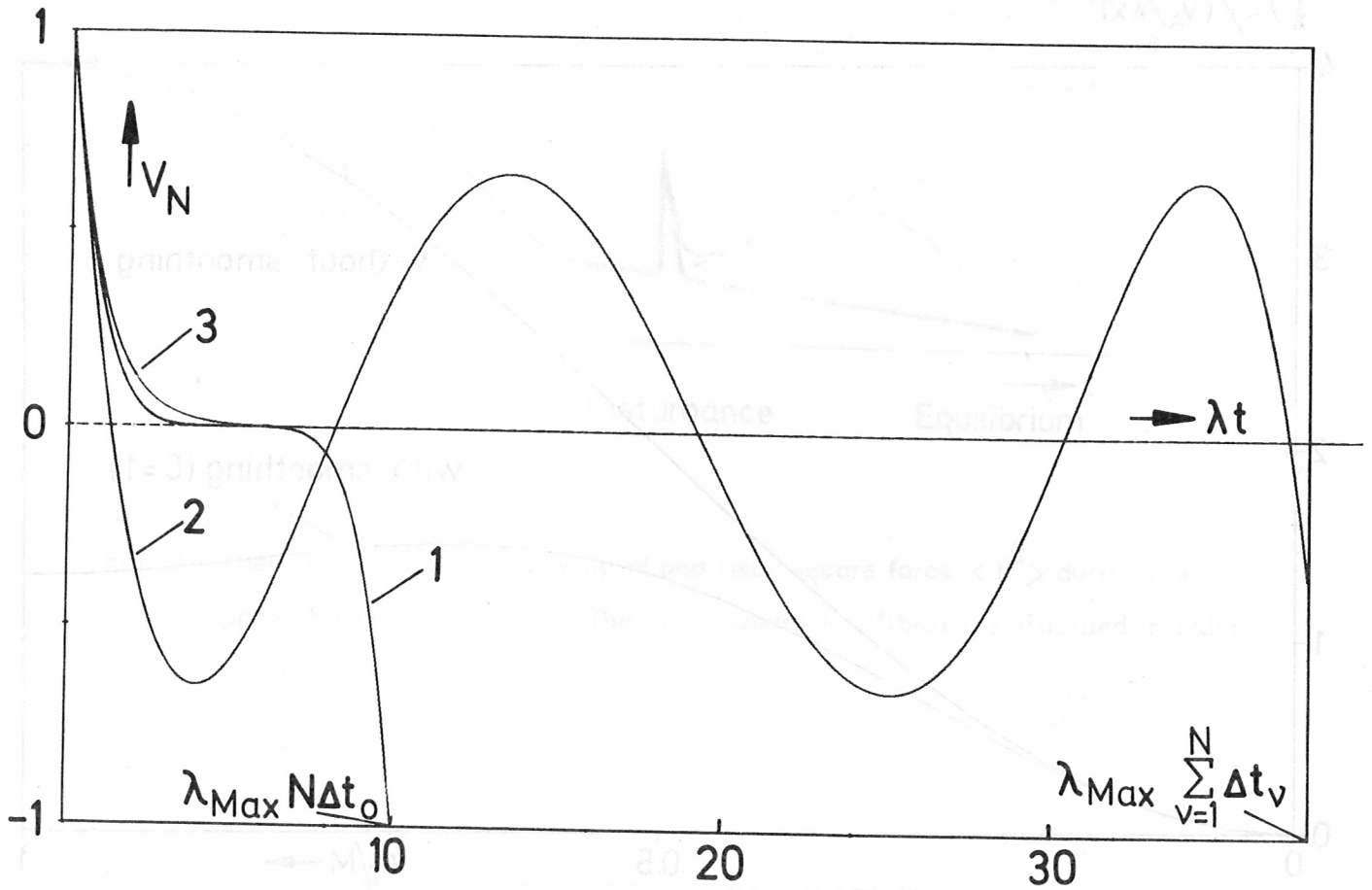
Fig. 6 Amplification factor V_N for a mode with eigenvalue λ

1. after N equal time steps $\Delta t_o = 2/\lambda_{Max}$, $t = N \Delta t_o$,

2. after N unequal optimized and relaxed time steps, $t = \sum\limits_{\nu=1}^{N} \Delta t_\nu = 18.9 \, \Delta t_o$
   for $N = 5$ and $\mathcal{E} = 0.02$

3. after a time t for the ideal case $\Delta t \to 0$.

Modes with small ("physical") eigenvalues are treated correctly, modes
with large ("numerical") eigenvalues are at least damped, $|V_N| \leqslant 1$.
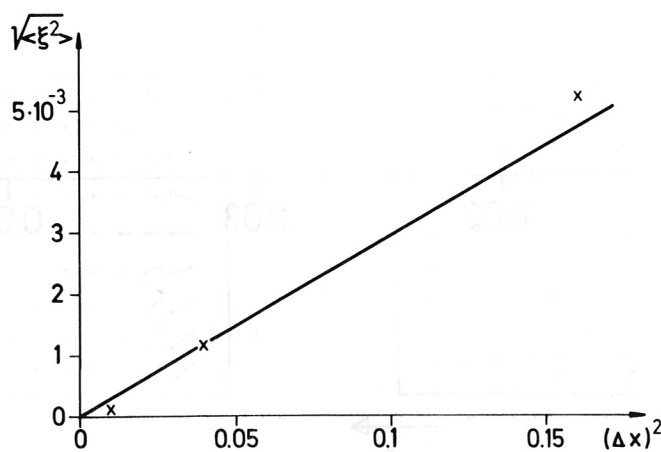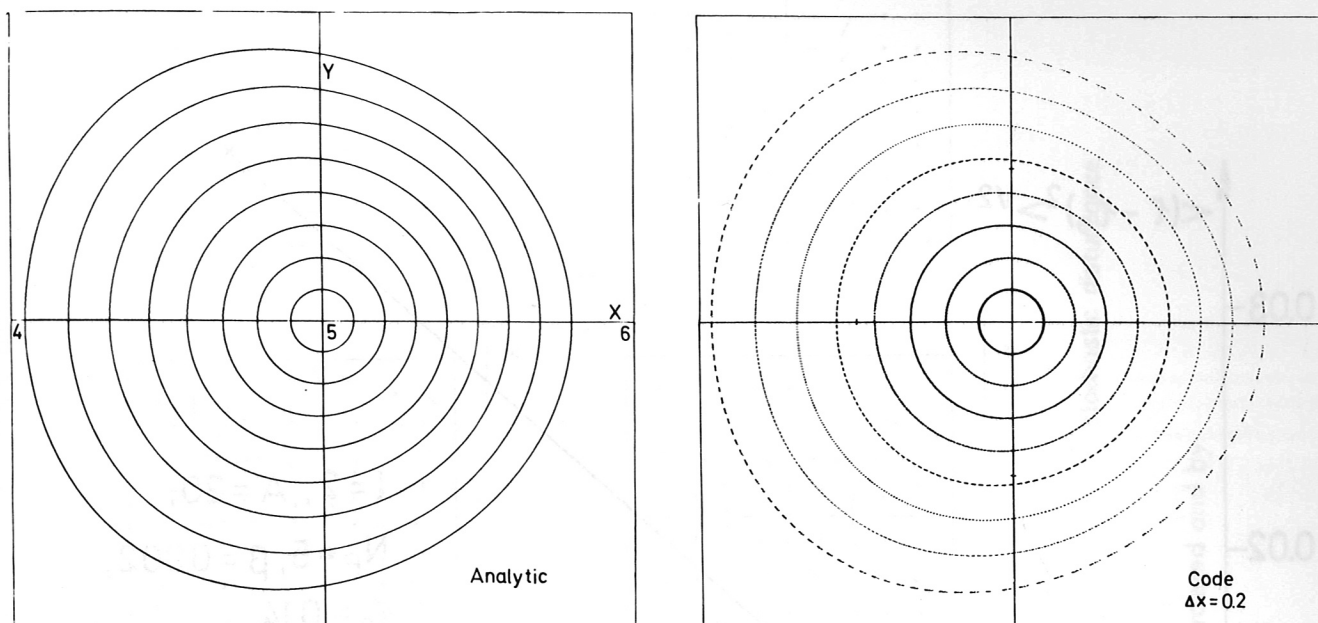
Fig. 7 Deviation ξ of the code from an analytic axisymmetric Solovev equilibrium for different mesh sizes Δx .
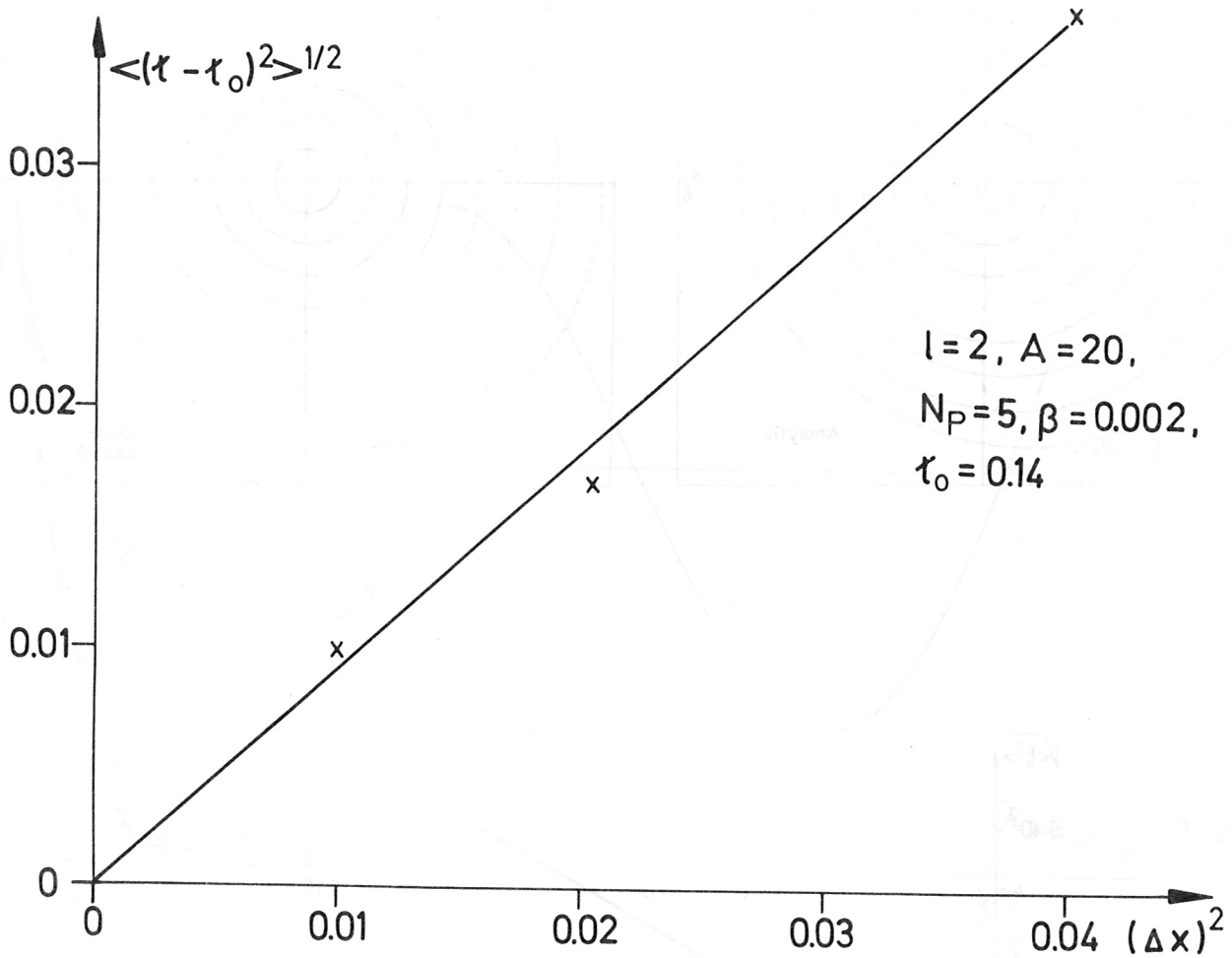
Fig. 8 R.m.s. change of rotational transform $\iota - \iota_o$ by flux loss during the shift of the magnetic axis in different grids. The configuration is the same as Fig. 11.

Excitation

final state

ordered disturbance
(m=2, n=1)

stochastic disturbance
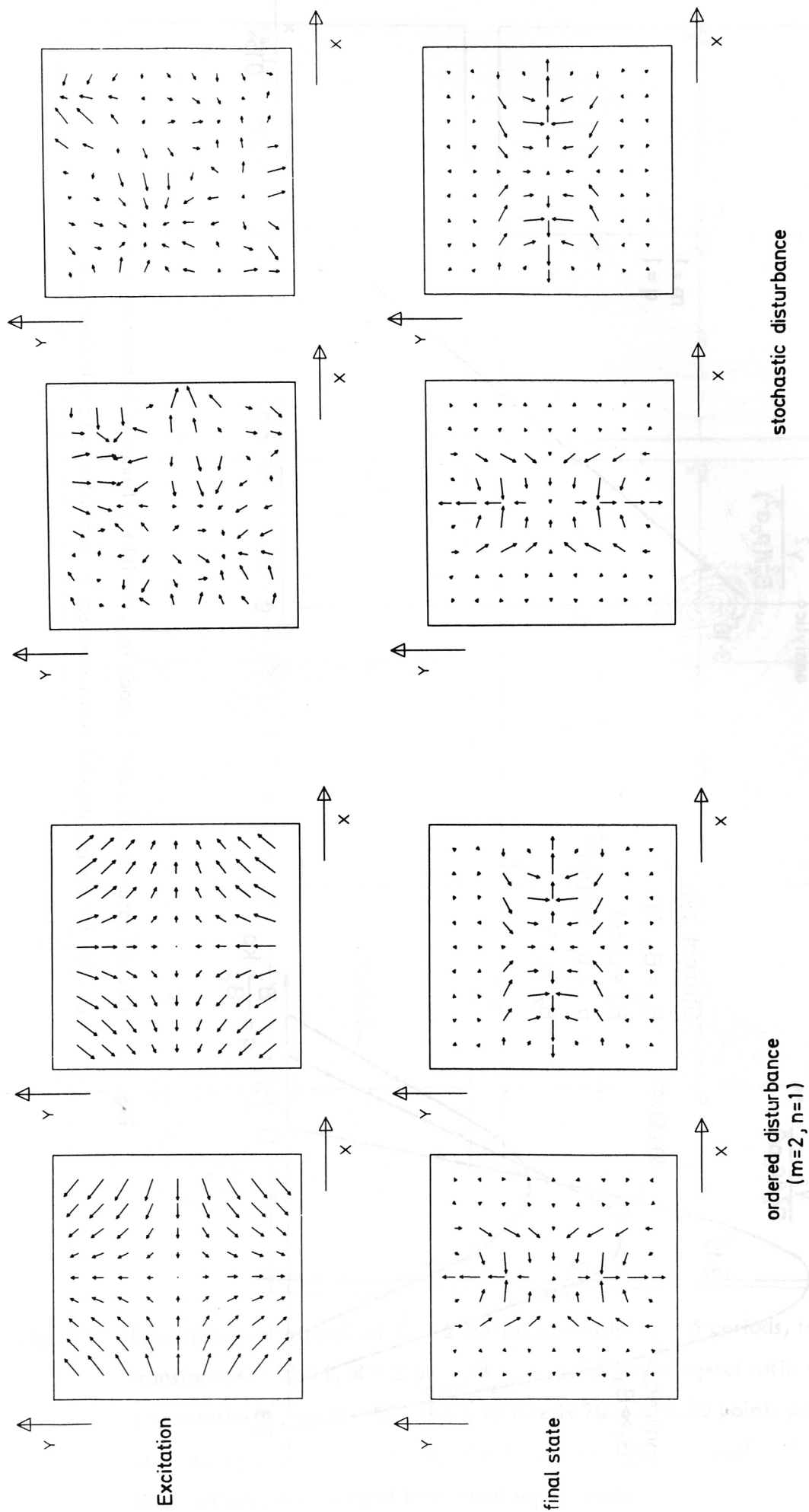
Fig. 9   Excitation of the lowest eigenvalue mode by an ordered and by
         a stochastic disturbance of an equilibrium.
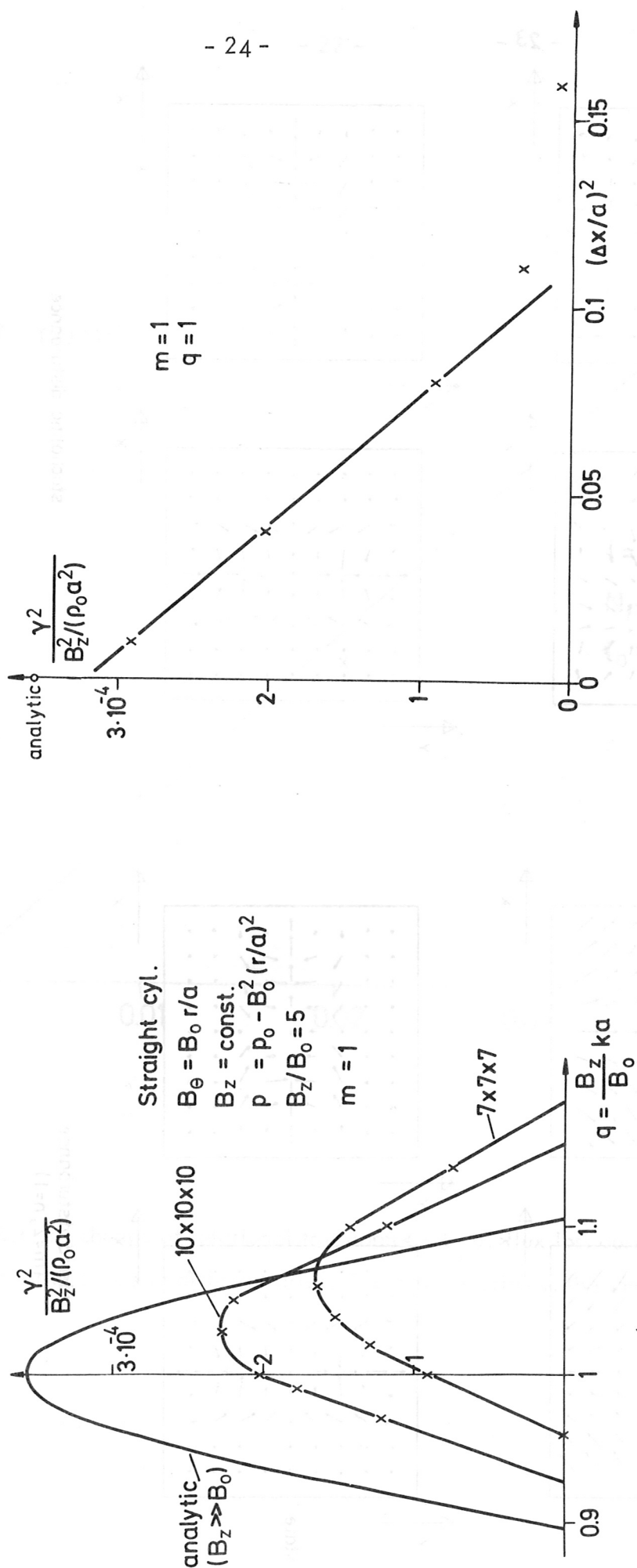
Fig. 10 Growth rates γ of a $m = 1$ mode in a straight cylinder with constant current density for different axial wave numbers k and different mesh sizes Δx.
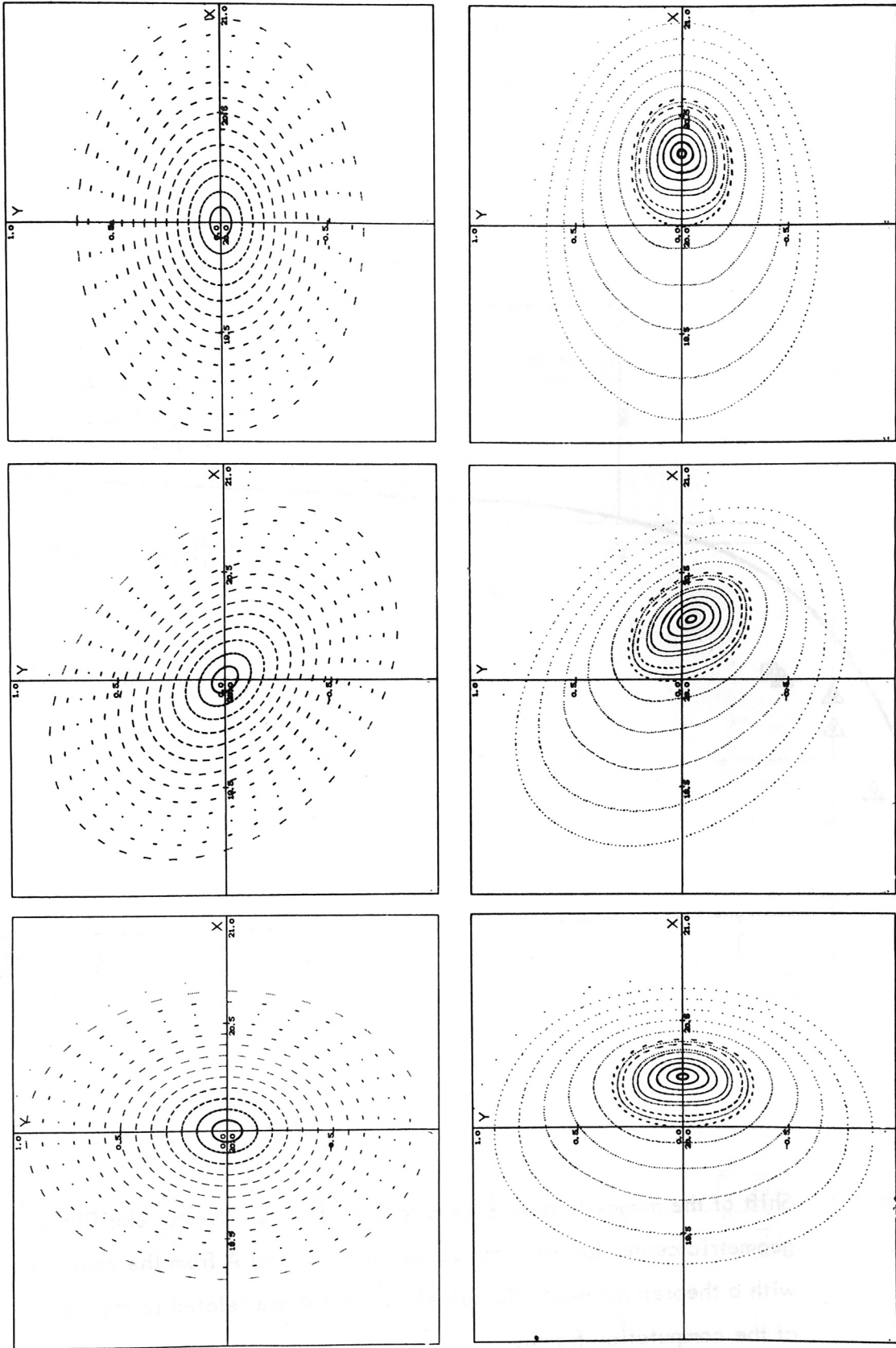
Fig. 11   Equilibrium of a toroidal $\ell = 2$ stellarator with $N_p = 5$ periods, total rotational transform $\ell = 0.14$, $\beta = 2\, p_{max}/B_{zo}^2 = 0.002$, and aspect ratio of the computation frame $A = 20$. The grid size is $20 \times 20 \times 20$ points per period. The figures show 3 cuts through the flux surfaces over a half period. First line: initial state; second line: final equilibrium.
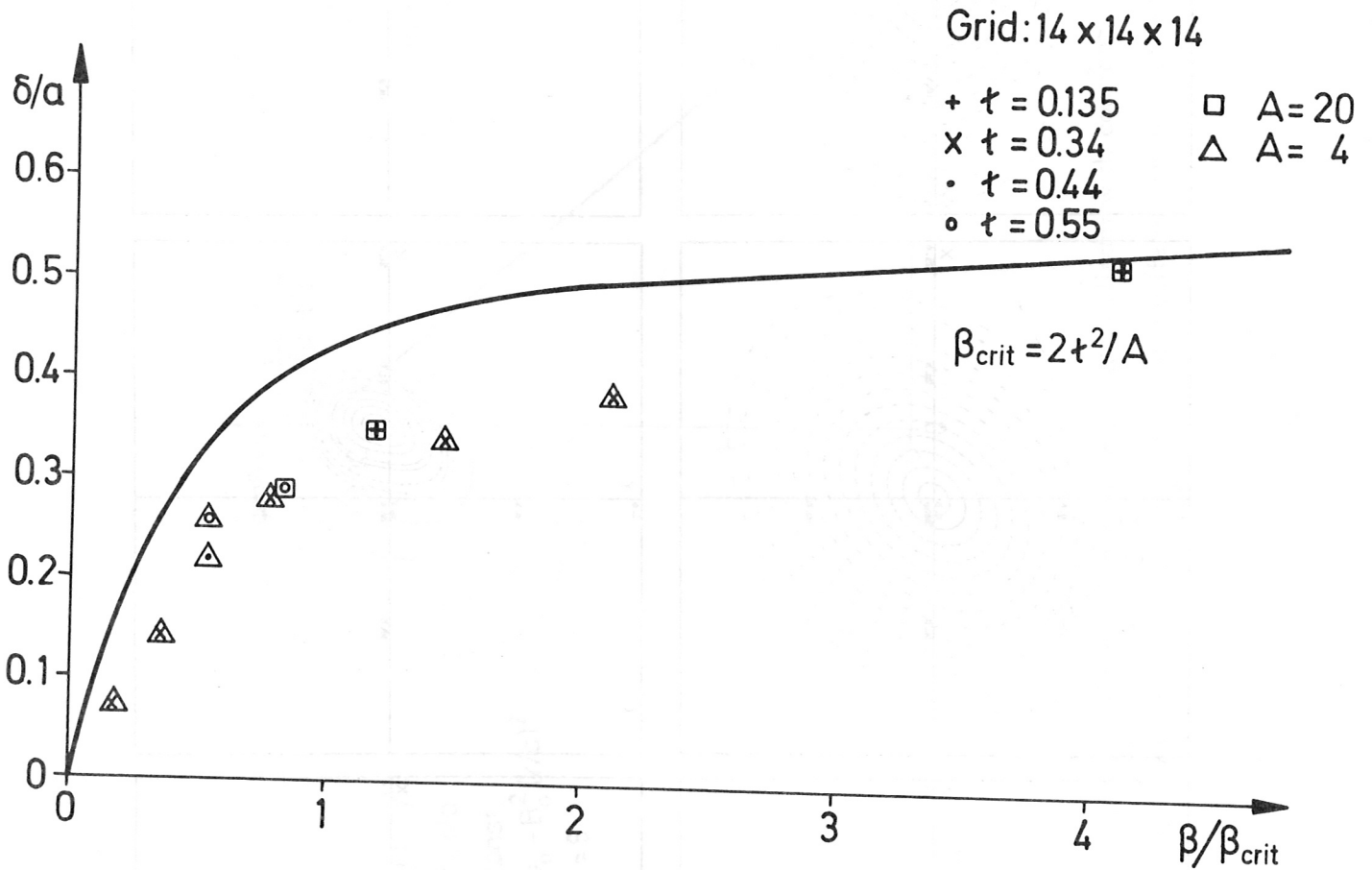
Fig. 12   Shift of the magnetic axis δ of a toroidal $\ell = 2$ stellarator equilibrium out of the geometric center for different values of β, t and A from the code together with a theoretical result (full line). δ and A are related to the half width of the computation frame.

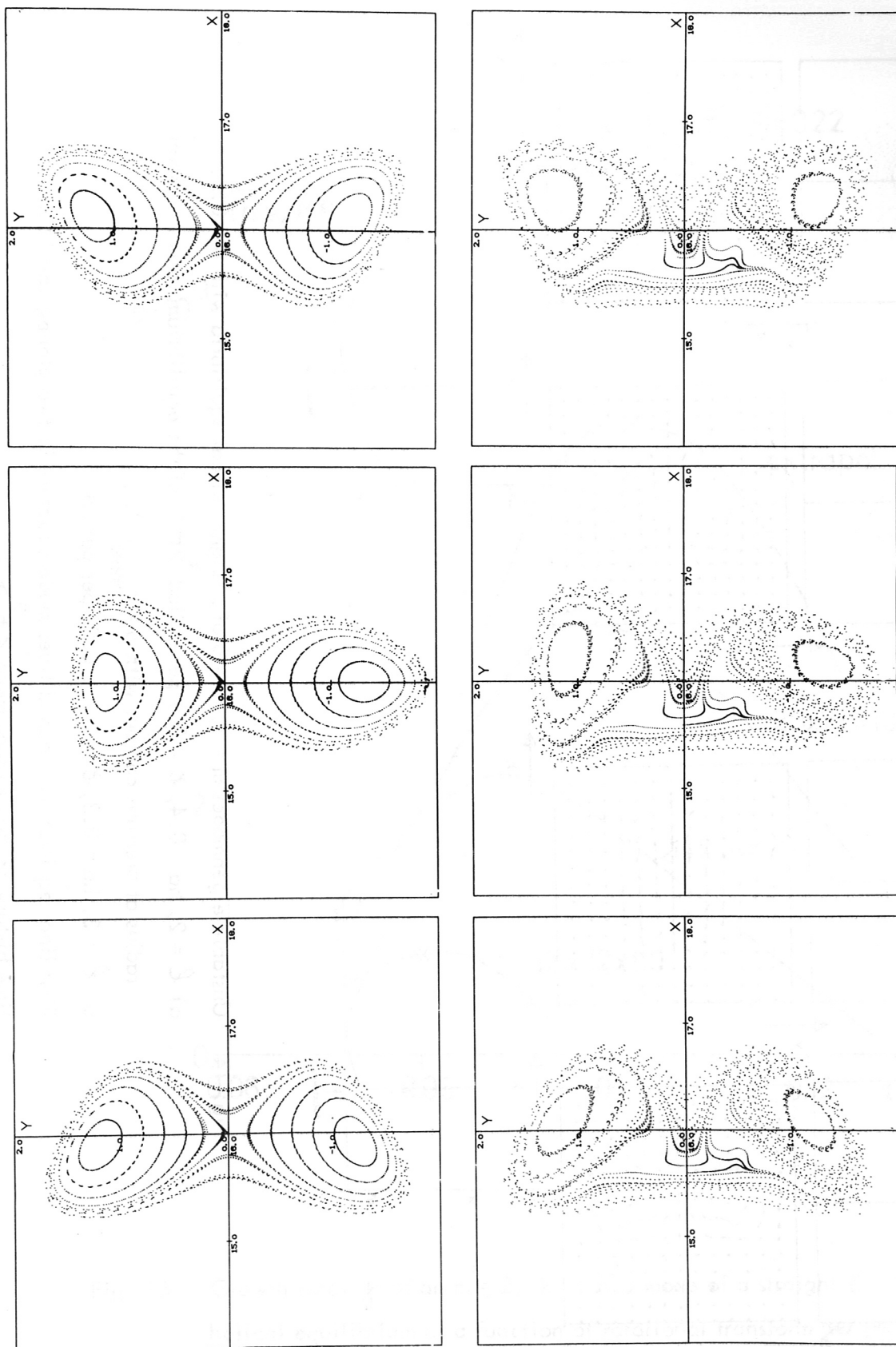Fig. 13　An equilibrium with two magnetic axes and a separatrix, $A = 16$, $N_p = 16$, $\beta = 0.03$ (first line: initial state; second line: final state).
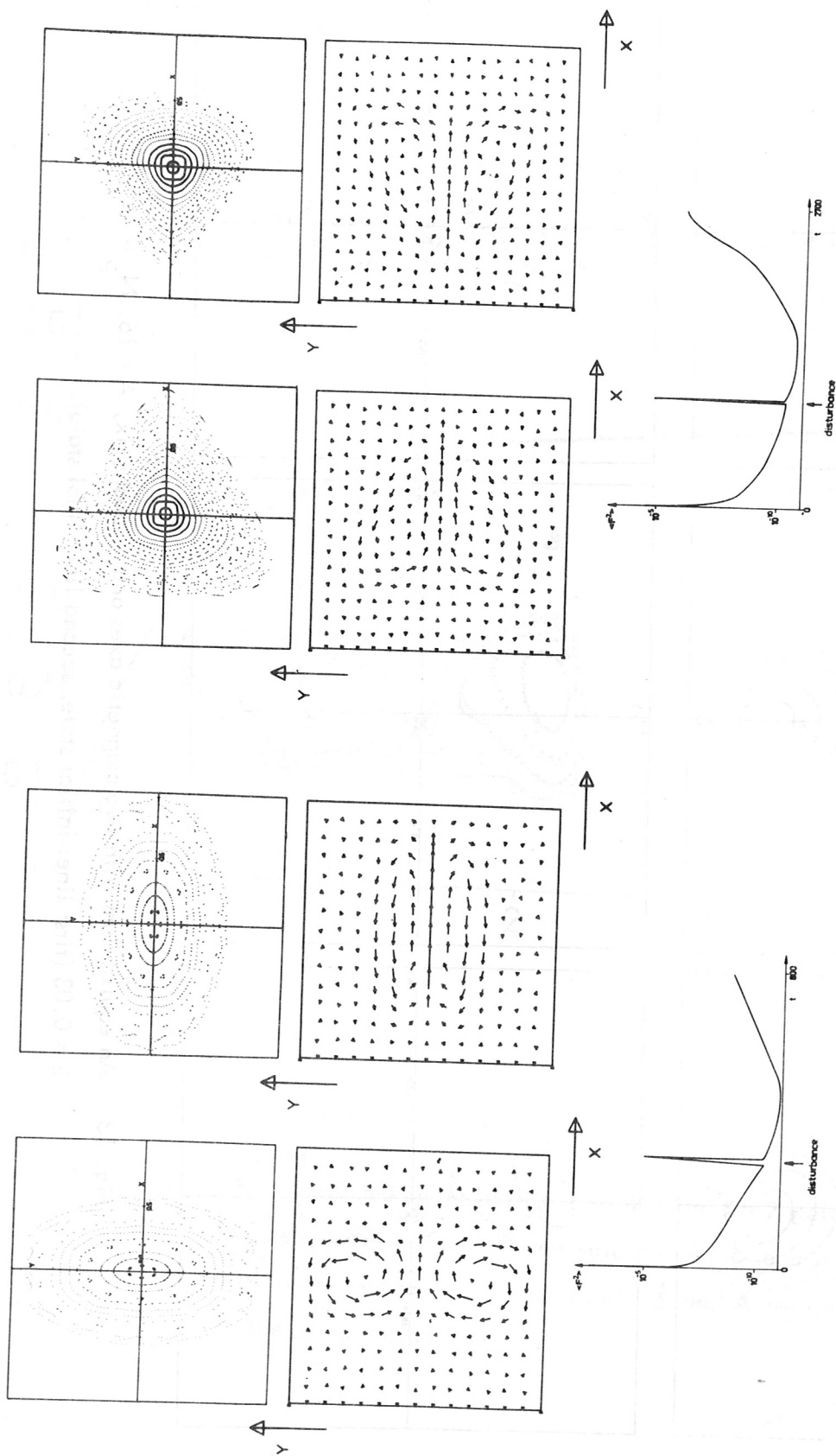
Fig. 14   Unstable eigenmodes m = 1, k = 0 of straight helical equilibria with ß = 0.5.

a) $\ell = 2$, ha = 0.4, $\iota = 0.1$ per period $2\pi/h$ of the equilibrium (a is the mean radius of pressure contour with $p = p_{max}/e$).

b) $\ell = 3$, ha = 0.3, $\iota = 0 \ldots 0.07$ per period.

First line: equilibrium; second line: mode structure in two planes; third line: time history of the residual force $\langle F^2 \rangle$.
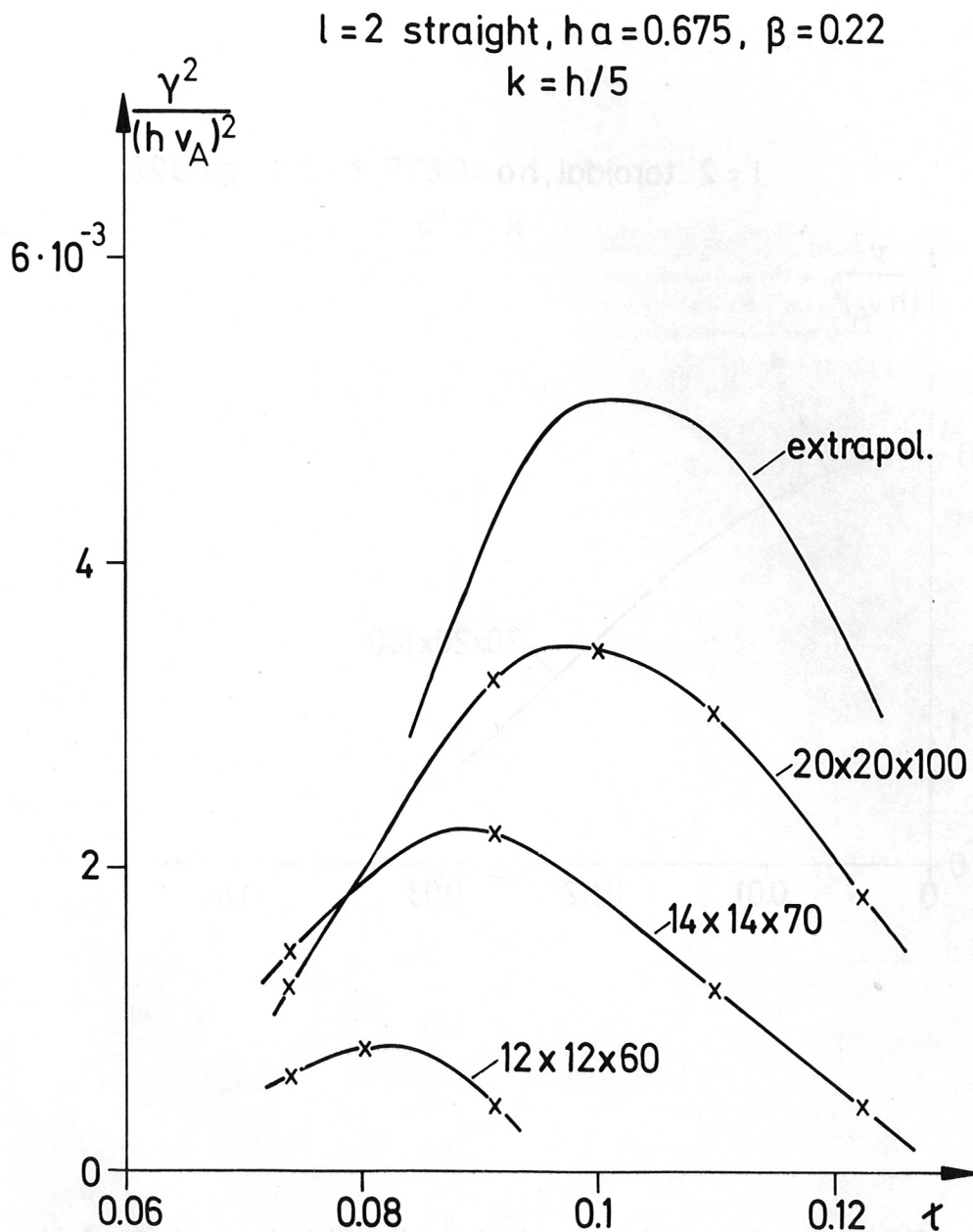
$$l = 2 \text{ straight}, \ ha = 0.675, \ \beta = 0.22$$
$$k = h/5$$

Fig. 15   Growth rates γ of an m = 2, k = h/5 mode of a straight ℓ = 2, ha = 0.675 helical equilibrium as a function of rotational transform per period t as caculated with different grids. The resonance should occur at t_{res} = 0.1.

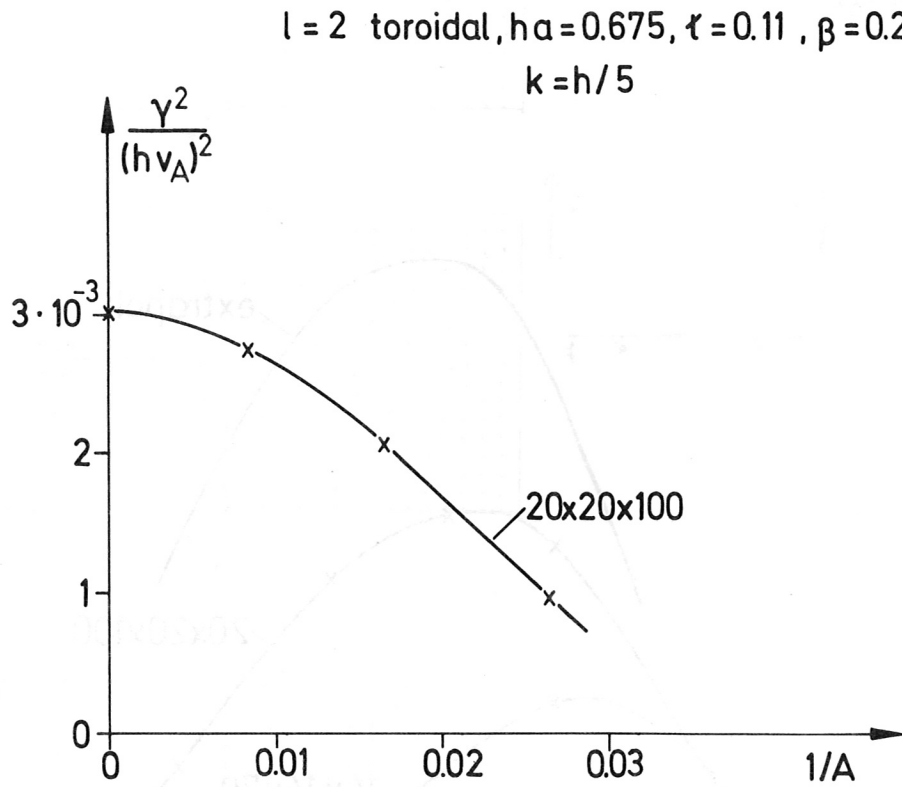Fig. 16   The same as Fig. 15 for a toroidal $\ell = 2$ equilibrium with $t = 0.11$ per period and varied plasma aspect ratios $A = n/(k\,a)$. n is the number of wavelengths of the disturbance along the torus, $N_p = 5n$.